AD-A101 979 NAVAL RESEARCH LAB WASHINGTON DC F/G 20/4
LAGRANGIAN SIMULATION OF TAYLOR-COUETTE FLOW.(U)
JUL 81 M H EMERY, M J FRITTS, R C SHOCKLEY
UNCLASSIFIED NRL-MR-4569 NL

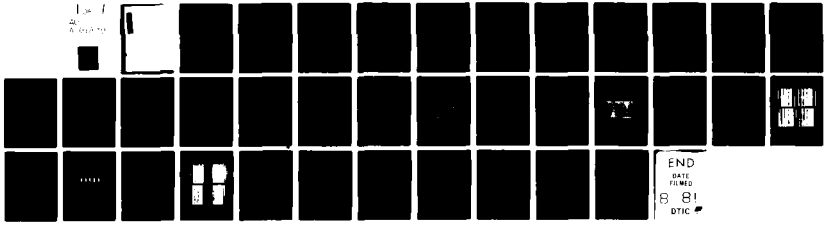

SECURITY CLASSIFICATION OF THIS PAGE (When Data Entered)

REPORT DOCUMENTATION PAGE	READ INSTRUCTIONS BEFORE COMPLETING FORM
1. REPORT NUMBER NRL Memorandum Report 4569 2. GOVT ACCESSION NO. AD-A101 979	3. RECIPIENT'S CATALOG NUMBER
4. TITLE (and Subtitle) LAGRANGIAN SIMULATION OF TAYLOR-COUETTE FLOW	5. TYPE OF REPORT & PERIOD COVERED Interim report on a continuing NRL problem. 6. PERFORMING ORG. REPORT NUMBER
7. AUTHOR(s) M.H. Emery, M.J. Fritts and R.C. Shockley*	8. CONTRACT OR GRANT NUMBER(s)
9. PERFORMING ORGANIZATION NAME AND ADDRESS Naval Research Laboratory Washington, D.C. 20375	10. PROGRAM ELEMENT, PROJECT, TASK AREA & WORK UNIT NUMBERS 61153N; RR0110941; 44-0574-01
11. CONTROLLING OFFICE NAME AND ADDRESS Office of Naval Research Washington, D.C.	12. REPORT DATE July 22, 1981 13. NUMBER OF PAGES 36
14. MONITORING AGENCY NAME & ADDRESS(if different from Controlling Office)	15. SECURITY CLASS. (of this report) UNCLASSIFIED 15a. DECLASSIFICATION/DOWNGRADING SCHEDULE

16. DISTRIBUTION STATEMENT (of this Report)

Approved for public release; distribution unlimited.

17. DISTRIBUTION STATEMENT (of the abstract entered in Block 20, if different from Report)

18. SUPPLEMENTARY NOTES

*Present address: Naval Ocean Systems Command, San Diego, CA.

19. KEY WORDS (Continue on reverse side if necessary and identify by block number)

Couette flow
Taylor vortex
Lagrangian
Triangular grid
Computational fluid dynamics

20. ABSTRACT (Continue on reverse side if necessary and identify by block number)

We report on the development of a hydrodynamics code designed for the Lagrangian simulation of transient rotational flow phenomena. The code solves the incompressible, inviscid fluid equations in an axisymmetric, cylindrical coordinate system. The equations of motion are finite differenced on a general connectivity triangular mesh. Here we apply the model to the study of the transition from laminar Couette flow to Taylor vortex flow and obtain very good agreement with the linear theory.

DD FORM 1 JAN 73 1473 EDITION OF 1 NOV 65 IS OBSOLETE
S/N 0102-014-6601

SECURITY CLASSIFICATION OF THIS PAGE (When Data Entered)

CONTENTS

LAGRANGIAN SIMULATION OF TAYLOR-COUETTE FLOW

I. Introduction

We report here on the development of the hydrodynamics code SPLASH which is designed for the Lagrangian simulation of transient rotational flow phenomena. The code solves the incompressible, inviscid fluid equations in an axisymmetric, cylindrical coordinate system. This is a 2 1/2 dimensional model with two spatial coordinates (r,z) and three velocity coordinates (u,w,v). All variables are independent of the angle θ.

The equations of motion are finite-differenced on a general-connectivity triangular mesh. A triangular mesh is the natural choice for flows in complicated geometries or flows with free surfaces or interfaces. The general-connectivity mesh allows local mesh restructuring whenever the grid distorts sufficiently to affect numerical accuracy and convergence. The SPLASH code is a direct extension of the hydrodynamics code SPLISH[1] which solves the incompressible, inviscid hydrodynamic equations on a triangular mesh in Cartesian geometry.

This model is applicable to a host of problems such as rotating columns of fluid including imploding liner systems with axially displaced annular or end plate pistons[2], axisymmetric jets, laser ablation of spherical shells and droplet combustion. Here we apply the model to the study of Couette flow and Taylor vortex[3] formation between two rotating coaxial cylinders. This problem was chosen as a test case because the linear theory is straightforward and well-developed[4,5] and there is a myriad of experimental results[6,7,8] available for comparison. We have been unable to find any numerical work in the literature which models the time-evolution of rotational flows to serve as a comparison.

Manuscript submitted May 14, 1981.

In the next section we discuss several aspects of the triangular gridding techniques. The equations of motion are developed in Section III with the finite-difference algorithms presented in Section IV. In Section V we discuss the Couette flow problem and the numerical results are presented in Section VI. The summary and conclusions make up Section VII.

II. Triangular Mesh

The set of equations governing incompressible, inviscid flow in a cylindrical coordinate system will be approximated by finite differences on a triangular mesh. The variables in these equations will be represented as triangle or vertex quantities on this mesh. This differencing procedure is somewhat complex. We will illustrate it by discussing some important basic concepts.

The basic computational cell is the shaded region shown in Fig. 1. It is formed by joining the side bisectors of the triangles surrounding the general vertex. Each triangle surrounding a central vertex contributes 1/3 of its area to the area of the basic cell.

We now illustrate how a gradient is represented in this model. If vertex quantities are linear functions of position, then, given the function g_m (defined on vertex m), the function g at any other point, n, say, can be written without approximation, as

$$g_n = g_m + \underline{R}_n \cdot \nabla g_n \qquad \text{(II-1)}$$

Here $\underline{R}_n$ is the vector from the location of g_m to the chosen point.

Now consider the triangle j defined by two side vectors $\underline{S}_i$, $\underline{S}_{i+1}$ with the vertex-defined quantities g, g_i and g_{i+1}. The index j indicates triangle quantities, the index i vertex quantities (see Fig. 2). Following

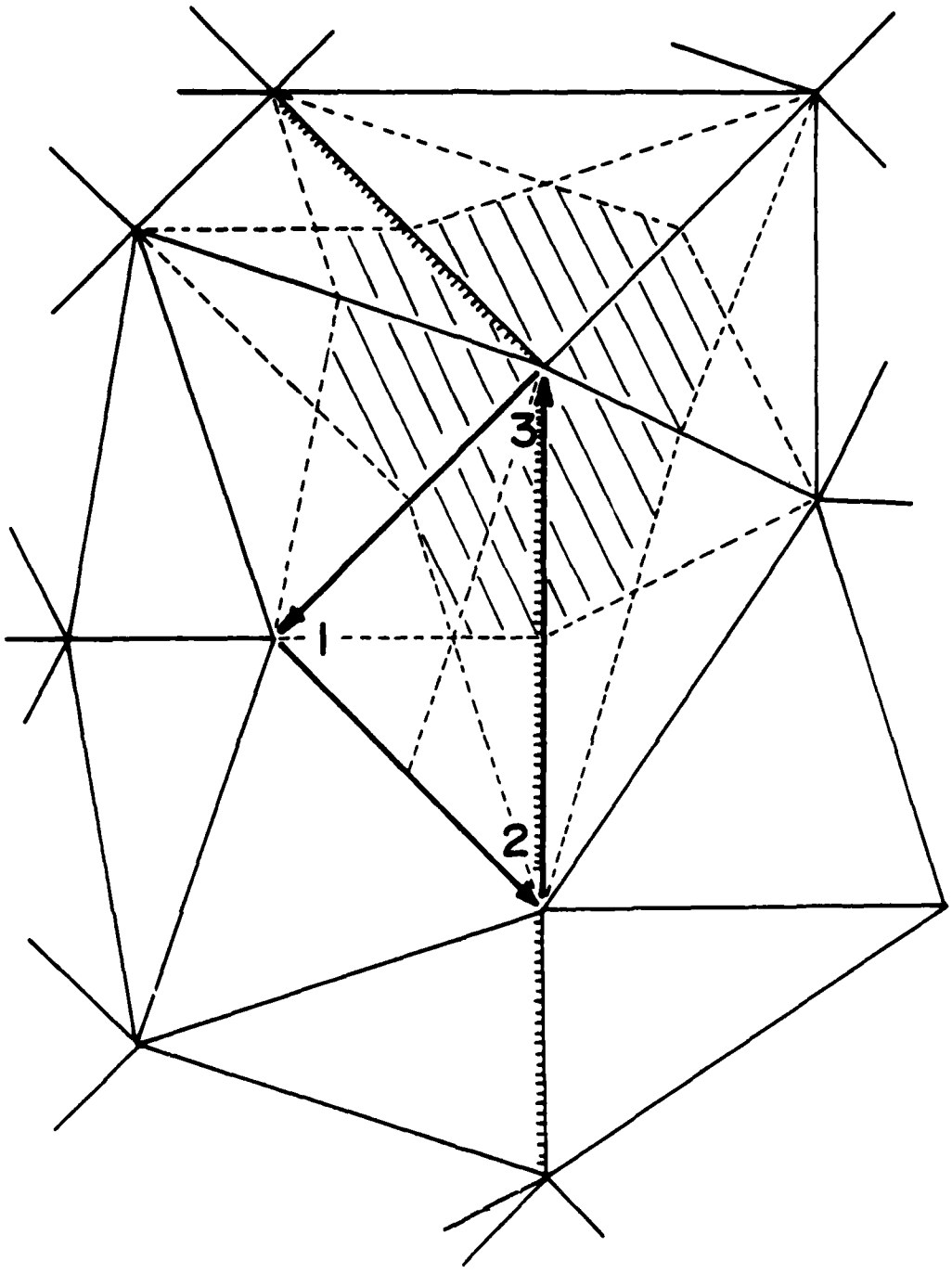

Fig. 1 — Detail of the triangular grid elements. A triangle is made up of three directed line segments, and a vertex represents the shaded region defined by the center of mass of each surrounding triangle and the midpoint of each side.

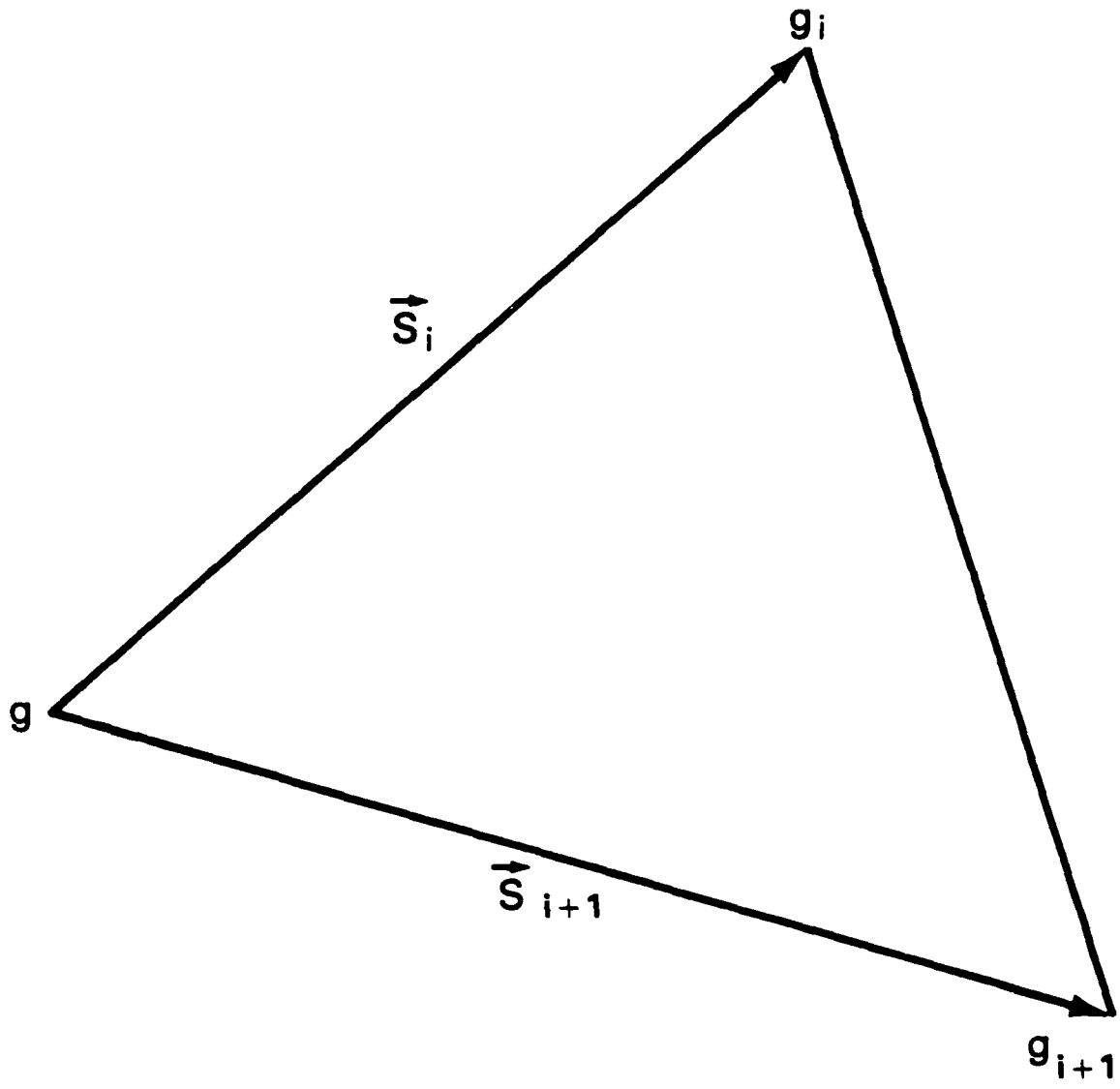

Fig. 2 — The gradient calculation. g is a vertex function. $\underline{S}_i$ and $\underline{S}_{i+1}$ are side vectors which define the triangle. ∇g is constant over the whole triangle.

Ref. 9, the gradient of g, uniquely defined on the triangle and constant throughout it is,

$$\nabla g_j = (g_i - g)\,\underline{s}^+_{i+1} - (g_{i+1} - g)\,\underline{s}^+_i$$

$$= \sum_{i=1}^{3} g_i \frac{\hat{n}\times(\underline{r}_{i-1} - \underline{r}_{i+1})}{2A_j} \qquad \text{(II-2)}$$

where $\underline{S}^+$ is the side vector $\underline{S}$ rotated clockwise by $\pi/2$ radians, and is shorthand for a cross product with a basis vector. Here n is a unit vector normal to the computational plane and A_j is the area of the triangle. $2A_j = (\underline{r}_{i+1} - \underline{r}_i) \times (\underline{r} - \underline{r}_{i+1}) \cdot \hat{n}$. $\underline{r}_i$ is the coordinate location of the vertex i. The conclusion is that gradients may be naturally represented on triangles, and easily calculated on them in the linear approximation.

The integral operator consists of a piecewise triangle summation about a basic cell giving rise to a vertex integral which is likewise exact for the linear approximation. Expressions for the divergence, curl and Laplacian are presented in detail in Ref. 1. The finite differencing of the nonlinear diffusion equation (Eq. A-5) is discussed in Ref. 10. Although the basic difference and integral operators are linear, the resulting weighting to a central vertex yields second order accurate approximations in the same way that central differences are second order accurate for one-dimension.

Although the control volume approach assures that the equations are solved conservatively, large numerical errors may arise in a Lagrangian code due to severe grid distortion. If portions of the grid become stretched, gradients will be calculated which involve vertices far removed from one another. The convergence of the iterations would be slow and truncation errors would build rapidly as the triangle sides lengthen.

This difficulty is avoided by forcing the mesh to restructure. Mesh restructuring may involve interchanging the diagonals of a quadrilateral formed by two adjacent triangles or adding/deleting a vertex on a triangle side or in the interior of a triangle. Restructuring is performed to preserve the diagonal dominance of the Poisson equation as a specific condition on the representational accuracy.

We employ the same basic restructuring algorithms as developed by Fritts[11] for Cartesian geometry. By conserving the linear momentum, circulation, divergence and the r and z components of the angular momentum on a quadrilateral (or triangle) a unique and reversible solution for the new r and z components of the triangle velocities is obtained. Conserving the θ component of the angular momentum and the generation of circulation gives rise to a unique solution for the new angular momentum. These reconnection algorithms will be discussed in more detail in a future report. In the next section we discuss the equations of motion.

III. Equations of Motion

The hydrodynamic equations of motion governing an incompressible, inviscid fluid in a cylindrical coordinate system (r, θ, z with corresponding velocity components u, v, w) are

$$\frac{\partial u}{\partial t} + u \frac{\partial u}{\partial r} + w \frac{\partial u}{\partial z} - \frac{v^2}{r} = - \frac{1}{\rho} \frac{\partial p}{\partial r} \quad , \tag{III-1}$$

$$\frac{\partial v}{\partial t} + u \frac{\partial v}{\partial r} + w \frac{\partial v}{\partial z} + \frac{vu}{r} = 0 \quad , \tag{III-2}$$

$$\frac{\partial w}{\partial t} + u \frac{\partial w}{\partial r} + w \frac{\partial w}{\partial z} = - \frac{1}{\rho} \frac{\partial p}{\partial z} \tag{III-3}$$

along with the incompressibility condition

$$\frac{1}{r}\frac{\partial}{\partial r}(ru) + \frac{\partial}{\partial z} w = 0 \quad . \tag{III-4}$$

Equation III-2 is just the conservation of angular momentum per unit mass. Defining the angular momentum per unit mass $L \equiv vr$, Equation III-2 is

$$\frac{\partial L}{\partial t} + \underline{u} \cdot \nabla L = \frac{dL}{dt} = 0 \quad . \tag{III-5}$$

We define a pseudo-Cartesian vector space with a gradient operator

$$\nabla' \equiv \hat{e}_r \frac{\partial}{\partial r} + \hat{e}_z \frac{\partial}{\partial z} \quad , \tag{III-6}$$

a vector velocity

$$\underline{u}' \equiv \hat{e}_r u + \hat{e}_z w \tag{III-7}$$

and a position vector

$$\underline{r}' \equiv \hat{e}_r r + \hat{e}_z z \quad . \tag{III-8}$$

Equation III-1 and III-3 can then be combined to give

$$\left(\frac{d}{dt}\right)' \underline{u}' = -\frac{1}{\rho} \nabla' p + \frac{v^2}{r} \hat{e}_r \quad , \tag{III-9}$$

where

$$\left(\frac{d}{dt}\right)' = \frac{\partial}{\partial t} + \underline{u}' \cdot \nabla' \quad .$$

Rewriting the r-component of Eq. III-9 we have

$$\rho \ddot{r} - \rho \frac{L^2}{r^3} = -\frac{\partial p}{\partial r} \quad .$$

This is precisely the equation of motion that would be obtained from a one dimensional Lagrangian

$$\mathcal{L} = \frac{1}{2} \rho \dot{r}^2 - \frac{1}{2} \rho \frac{L^2}{r^2} - p \tag{III-10}$$

with a potential

$$V = p + \frac{1}{2}\rho\frac{L^2}{r^2} \quad . \tag{III-11}$$

The equations of motion in our pseudo-Cartesian coordinate system become

$$(\frac{d}{dt})'L = 0$$

and the angular momentum of a fluid element, per unit mass, remains constant as we follow it with its motion; and

$$(\frac{d}{dt})'\underline{u}' = -\frac{1}{\rho}\nabla' p - \frac{1}{2}L^2\nabla'\frac{1}{r^2} \quad . \tag{III-12}$$

The radial and axial motion takes place as if v were absent and, instead, a centrifugal force, $F_{\underline{c}} = -\rho\frac{1}{2}L^2\nabla'\frac{1}{r^2}$, were acting in the radial direction. Note that the angular momentum is constant in the region over which the gradient is applied. It is therefore a triangle quantity -- the basic fluid element in this code -- and each triangle resides in a $1/r^2$ potential. The incompressibility condition takes the form

$$\nabla' \cdot (r\underline{u}') = 0 \quad . \tag{III-13}$$

Equations III-11, 12, 13 now have the same formulation as the Cartesian version of the code (SPLISH). The finite-difference algorithms and the restructuring algorithms developed for SPLISH can then be applied to cylindrical geometry with modifications to include conservation of vorticity generation and conservation of angular momentum. The pseudo-Cartesian coordinate system will be utilized throughout the remainder of this paper. For that reason the primed notation will be dropped in what follows. In the next section we discuss the finite-difference algorithms.

IV. Finite-Difference Algorithms

The computer code SPLASH is a 2 1/2-dimensional Lagrangian fluid dynamics code for incompressible fluids in cylindrical geometry. This code is a direct extension of the philosophy and numerical techniques developed for SPLISH, the Cartesian version of the code. As such, most remarks in this section apply equally as well to SPLISH.

The basic equations are,

$$\rho \frac{d\underline{u}}{dt} = -\nabla p - \rho \frac{L^2}{2} \nabla \frac{1}{r^2} \quad , \tag{IV-1}$$

$$\nabla \cdot (r\underline{u}) = 0 \tag{IV-2}$$

and

$$\frac{dL}{dt} = 0 \quad . \tag{IV-3}$$

The fluid density ρ, pressure p, angular momentum L and velocity $\underline{u}$ are assumed to vary only with r and z. With pressures specified at the verticies, ∇p is evaluated over triangles, and Eq. IV-1 can easily be updated implicitly or explicitly if velocities are considered to be triangle-centered. This placement of velocities as cell quantities and pressures at vertices is apparently unique to SPLASH and SPLISH and is the direct opposite of the usual placement. In what follows the subscript i will denote a vertex-centered quantity and j a triangle-centered quantity. In both codes the integration of velocities uses a split step algorithm whereby the velocities are advanced one half timestep (Eq. IV-4), the grid is advanced a full timestep (Eq. IV-6) and then the velocities advanced forward the other half timestep (Eq. IV-8)

$$\underline{U}_j^{\frac{1}{2}} = \underline{U}_j^o - \frac{\delta t}{2 v_j} (\nabla p)_j^o - \frac{\delta t}{2} \frac{L_j^2}{2} \left(\nabla \frac{1}{r^2}\right)_j^o \tag{IV-4}$$

$$\underline{U}_i^{\frac{1}{2}} = \frac{1}{2} (\underline{U}_i^o + \underline{U}_i^n) \quad , \tag{IV-5}$$

$$\underline{R}_i^n = \underline{R}_i^o + \delta t \underline{U}_i^{\frac{1}{2}} \quad , \tag{IV-6}$$

$$\tilde{\underline{U}}_j = \underline{\underline{R}}[(\underline{R}_i^o), (\underline{R}_i^n)] \cdot \underline{U}_j^{\frac{1}{2}} \quad , \tag{IV-7}$$

$$\underline{U}_j^n = \tilde{\underline{U}}_j^{\frac{1}{2}} - \frac{\delta t}{2\rho_j} (\nabla p)_j^n - \frac{\delta t}{2} \frac{L_j^2}{2} (\nabla \frac{1}{r^2})_j^n \tag{IV-8}$$

The vertex velocity $\underline{U}_i^n$ appearing in Eq. IV-5 is obtained from the area-weighted $\underline{U}_i^n$ from the previous iteration,

$$\underline{U}_i^n = \frac{\sum_j \underline{U}_j^n A_j}{\Sigma A_j} \tag{IV-9}$$

The advantage of using triangle centered velocities is the ease in conceptualizing and expressing conservation laws. Because of the paucity of experience in formulating algorithms over a general triangular grid, we employed a control volume approach, which uses an integral formulation to derive the difference algorithms. Equation IV-7 is the first manifestation of this approach. It reflects numerically the fact that the triangle velocities must rotate and stretch as the grid rotates and stretches. The transformation $\underline{\underline{R}}$ is derived by considering the circulation about each vertex. The boundaries of a vertex cell are defined by the triangle side bisectors as noted in Section II.

The vertex of Fig. 1 is constructed by summing over all the surrounding triangles. Therefore the area of a vertex cell may be defined as

$$A_c = \sum_j \frac{1}{3} A_j \quad , \tag{IV-10}$$

where the sum extends over all adjacent triangles. With this definition the vertex velocity becomes

$$\underline{U}_i = \frac{\frac{1}{3}\sum_j \underline{U}_j A_j}{A_c} \quad . \tag{IV-11}$$

Since the triangle velocities are constant over the triangle, the circulation taken about the boundary of the vertex cell is straightforward. Circulation is conserved about each of the three triangle vertices by the transformation $\underline{\underline{R}}$ of Eq. IV-7. This transformation ensures that the vorticity integral calculated about any interior vertex is invariant under the advancement of the grid. It is easy to show that the ∇p term cannot alter the vorticity either since numerically $\nabla\times\nabla p \equiv 0$. Only the $(\nabla p_j/\rho_j)$ and $\left(L^2/2\ \nabla\frac{1}{r^2}\right)$ terms can change vorticity, exactly as dictated by the physics. Since the transformation $\underline{\underline{R}}$ is time reversible, so are Eqs. IV-4 - IV-8, so that the entire algorithm advances vertex positions and velocities reversibly while evolving the correct vorticity about every interior vertex. No numerical generation of nonphysical vorticity can occur, a rather unique feature of both SPLASH and SPLISH among Lagrangian codes.

The pressure p_i^n in Eq. IV-8 is derived from the condition that the new velocities $\underline{U}_j^n$ should be divergence free at the new timestep, satisfying Eq. IV-2. The pressure Poisson equation is derived from Eq. IV-8 by setting $(\nabla\cdot r_j\underline{U}_j^n)_i \equiv 0$, to obtain pressure p_i^n such that

$$\frac{\delta t}{2}\left[\nabla\cdot\frac{r_j}{\rho_j}(\nabla p)_j^n\right]_i = (\nabla\cdot r_j\underline{\tilde{U}}_j^{\frac{1}{2}})_i - \frac{\delta t}{2}\nabla\cdot\left[\frac{r_j L_j^2}{2}(\nabla\frac{1}{r^2})_j^n\right]_i \quad , \tag{IV-12}$$

where

$$r_j = \frac{1}{3}\sum_{i=1}^{3} r_i \quad .$$

Both terms in Eq. IV-12 are simple to evaluate since the divergence is taken over triangle centered quantities. The paths are the "surfaces" bounding the vertex volume of Fig. 1, where the normal is directed outward from the vertex. The Poisson equation (Eq. IV-12) that results from this integration has two advantages. First it is derived from $\nabla^2\phi = \nabla\cdot\nabla\phi$ as in the continuum case. Secondly the left-hand side results in the more familiar second order accurate templates (such as the five-point formula) for the Laplacians for homogeneous fluids and regular mesh geometries.

In summary the finite difference formulas for SPLASH are derived using a control volume approach. Specifications of pressure at vertices leads naturally to the choice of positioning velocities at triangles. Although pressure gradients are constant over triangles, the resultant algorithms are expected to be nearly second order accurate since vertex velocities are derived from pressure gradient forces through sums about vertices, which in effect centralizes the differences. SPLISH has been tested extensively on finite amplitude standing waves and has been shown to be basically second-order accurate by studying the variation in period with mesh size.[1,12]

V. Couette Flow

Couette flow refers to the circular flow of a fluid between two rotating coaxial cylinders. This flow is potentially unstable; the instability results from a prevailing adverse gradient of angular momentum.

The stability of an ideal fluid in circulatory motion was first investigated by Rayleigh.[13] Simply stated, Rayleigh's criterion says that in the absence of viscosity, the necessary and sufficient condition for a distribution of angular velocity $\Omega(r)$ to be stable is

$$\frac{d}{dr}(r^2\Omega)^2 > 0$$

everywhere in the interval and that the distribution is unstable if $(r^2\Omega)^2$ should decrease anywhere in the interval.

Note that $r^2\Omega$ is the angular momentum, per unit mass, of a fluid element about the axis of rotation. We have shown in Section III that the angular momentum of an ideal fluid element is a constant of the motion and that the motions along the radial and axial direction may be treated as if the circulatory motion were absent and instead a centrifugal force $[-\rho L^2/2\forall(1/r^2)]$ were acting in the radial direction. Thus we may associate with each fluid element a "potential energy" $\rho L^2/2r^2$. This is analogous to the problem of a heterogeneous fluid in a field with a potential energy proportional to r^{-2}. The equilibrium is stable only if the potential energy is a minimum; i.e., the "heavier" fluids are in regions of lower potential energy. This means that L^2 must be monotonically increasing outwards.

Taylor[3] extended this criterion for stability to account for viscosity, verified his calculations experimentally and described the secondary flow which appears after the onset of the instability. Viscosity tends to produce an angular momentum distribution proportional to Ar^2+B for laminar Couette flow, where A and B are two constants related to the angular velocities of the inner and outer cylinders. If this distribution is unstable, fluid elements with larger angular momenta will move outwards inducing a secondary flow. Viscous forces will tend to retard this motion but if a viscous drag is not strong enough a redistribution of angular momentum will occur. At the same time, the moving solid surfaces will tend to re-establish the original distribution of vorticity and a steady secondary flow is established. This secondary flow consists of a regular

cellular vortex structure in which closed ring vortices alternating in sign are wrapped around the axis of symmetry.

The transiton from steady, laminar Couette flow into fully developed Taylor vortex flow is the phenomenon we are simulating here. To obtain a quantitative comparison with theory, we compare the growth rates of the instability with those obtained from the linear theory developed by Chandrasekhar.[4]

Following Chandrasekhar, we linearize the equations of inviscid motion (Eqs. III-1 - III-4) by doing a perturbation expansion about the stationary flow solution

$$u = \varepsilon u^{(1)} + \varepsilon^2 u^{(2)} + \ldots$$

$$w = \varepsilon w^{(1)} + \varepsilon^2 w^{(2)} + \ldots$$

$$v = V^o(r) + \varepsilon v^{(1)} + \varepsilon^2 v^{(2)} + \ldots$$

and $$p = p^o(r) + \varepsilon p^{(1)} + \varepsilon^2 p^{(2)} + \ldots$$

where $V^o(r) = r\Omega(r)$. Assuming all perturbed quantities vary as $\exp[i(\sigma t + kz)]$ where σ is a constant (which can be complex) and k is the wave number of the disturbance in the z-direction, we have to first order

$$i\sigma u^{(1)} = 2\Omega v^{(1)} - \frac{1}{\rho}\frac{\partial}{\partial r} p^{(1)} \quad , \tag{V-1}$$

$$i\sigma v^{(1)} + \left[\Omega + \frac{\partial}{\partial r}(r\Omega)\right] u^{(1)} = 0 \tag{V-2}$$

$$i\sigma w^{(1)} = -\frac{ik}{\rho} p^{(1)} \tag{V-3}$$

and $$\frac{\partial u^{(1)}}{\partial r} + \frac{u^{(1)}}{r} + ikw^{(1)} = 0 \quad . \tag{V-4}$$

combining Eqs. V-1 and V-2 and Eqs. V-3 and V-4 and eliminating the pressure between the resulting two equations we have (dropping superscripts)

$$\frac{\partial}{\partial r}\left[\frac{1}{r}\frac{\partial}{\partial r}(ru)\right] = (k^2/\sigma^2)[\sigma^2 - \Phi(r)]u \qquad \text{(V-5)}$$

where

$$\Phi(r) = \frac{2\Omega}{r}\ \frac{\partial}{\partial r}\ (r^2\Omega) \quad ,$$

along with the boundary conditions on the inner (R_1) and outer (R_2) cylinders

$$u(R_1) = u(R_2) = 0 \quad .$$

Since the numerical code is Lagrangian, we rewrite Eq. V-5 in terms of Lagrangian displacement variable ξ[4]

$$u = i\sigma\xi_r$$

$$v = i\sigma\xi_\theta - r\,\frac{d\Omega}{dr}\,\xi_r$$

$$w = i\sigma\xi_z \quad .$$

We also express the angular velocity in terms of its viscid distribution $\Omega(r) = A + B/r^2$. Equation V-5 then takes the form

$$(DD_*-k^2)\xi_r = -\frac{4k^2}{\sigma^2}A(A+B/r^2)\xi_r \qquad \text{(V-6)}$$

where

$$D = \frac{d}{dr} \quad \text{and} \quad D_* \quad \frac{d}{dr} + \frac{1}{r}$$

and the boundary conditions are

$$\xi_r = 0 \text{ at } r = R_1,\ R_2.$$

Equation V-6 can be solved explicitly in terms of Airy functions for the case of a small gap[14]

$$d = (R_1 + R_2) << 1/2(R_1 + R_2).$$

The solutions are complicated in that the wavenumber and growth rate are linked parametrically. The coupling terms in the pair of resulting equations are determined from a characteristic equation expressed as a ratio of Airy functions. We use the growth rates of the most unstable mode as determined by Reid[14] and Chandrasekhar[4] to compare with the numerical simulation.

VI. Numerical Results

The initial grid for the Couette flow simulation is shown in Fig. 3. $R_1(R_2)$ is the radius of the inner (outer) cylinder. $z_o(z_N)$ is the left (right) boundary of the computational region. The θ coordinate is into the page. The boundary conditions are

$$u(R_1) = u(R_2) = 0 \quad ,$$

and the system is periodic in the z-direction

$$z_o = z_{N+1} \quad , \qquad \rho(z_o) = \rho(z_{N+1}),$$

$$w(z_o) = w(z_{N+1}) \qquad p(z_o) = p(z_{N+1})$$

and

$$u(z_o) = u(z_{N+1}) \quad .$$

The initial angular velocity is assumed to have the viscid distribution

$$\Omega(r) = A + B/r^2$$

where A and B are constants which depend on the angular frequency of the inner and outer cylinders. The system is initially in equilibrium with a pressure distribution given by

$$p^o(r,z,t=0) = \rho \int_{R_1}^{r} \frac{v^2(r,z)}{r}\, dr + C$$

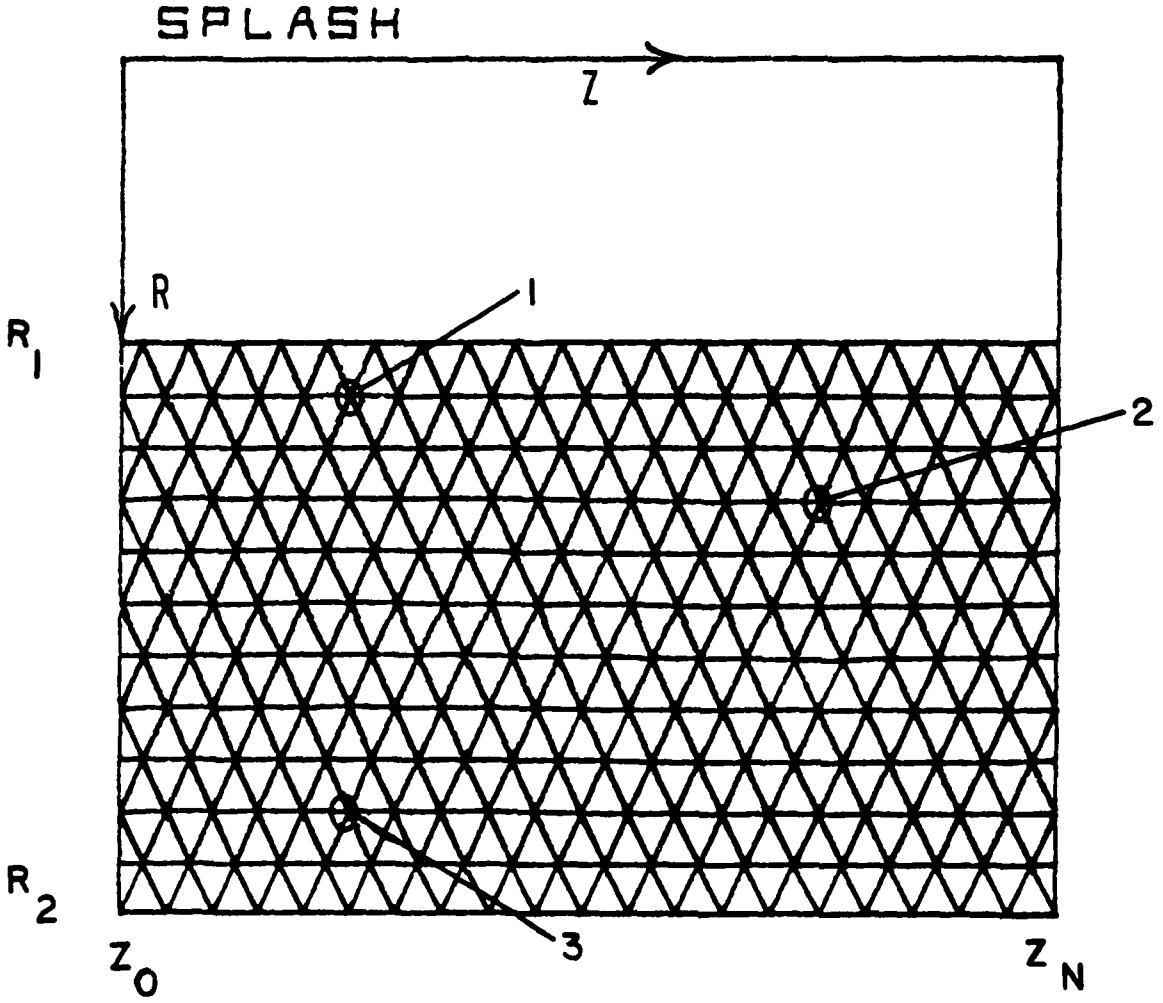

Fig. 3 — The initial computational grid for the Taylor-Couette problem. The θ-direction is into the paper. $R_1(R_2)$ is the radius of the inner (outer) cylinder. The r-component of velocity for vertices 1, 2 and 3 are followed in time.

where C is an arbitrary constant except in the case of a free surface at the inner cylinder when it is zero.

This initial pressure distribution is then perturbed with a 1% sinusoidal perturbation,

$$p'(r,z,t=0) = p^{o}(r,z,t=0) + 0.01p^{o}(r,z,t=0) \sin kz$$

where k is the wavenumber of the most unsable mode. The most unstable mode is the mode for which the Taylor vortices have a wavelength equal to twice the gap width, i.e., the vortices are approximately square in cross-section.

Two important parameters governing the stability or instability of Couette flow are the ratio of radii of the inner and outer cylinders

$$\eta = R_1/R_2 \quad ,$$

and the ratio of the angular frequencies of the outer and inner cylinders

$$\mu = \Omega_2/\Omega_1 \quad .$$

The Rayleigh criterion for stability can then be written as

$$\mu > \eta^2 \quad .$$

For all the results presented here, the small gap approximation is valid.

For Case I we have

$$R_1 = 21 \text{ cm}, \; R_2 = 23 \text{ cm},$$

$$z_N = 4 \text{ cm}, \; k = 2\pi/\lambda = \pi/2$$

and

$$\Omega_1 = 40\pi \text{ sec}^{-1}, \; \mu = 1/2 \; ,$$

and this system is unstable since $\mu < \eta^2$. The initial grid is shown in Fig. 3 where we have denoted three vertices which we will follow in time.

Figure 4 shows the system shortly after one full revolution. As one would expect the fluid near the inner cylinder with its larger angular momentum is being pushed to a larger radius and the fluid near the outer cylinder with its smaller angular momentum is being pushed to a smaller radius, i.e., the "heavy" fluid is falling and the "light" fluid is rising. Note the large number of vertices that have been added near the boundaries to preserve the resolution there.

The time evolution of the r-component of velocity for the three aforementioned vertices is shown in Fig. 5. The growth rates for the three vertices are equal for nearly a full revolution at which point vertex 1 slows down and vertices 2 and 3 speed up. The growth rate in the linear regime $\gamma_c = 213.09\ s^{-1}$ is in very good agreement with the predicted growth rate $\gamma_t = 215.26\ s^{-1}$ obtained from linear theory.

Vertices 2 and 3 are speeding up because they are becoming entrained between two very large counter-rotating vortices. Vertex 1 is nearing the inner cylinder and being deflected in the z-direction. This is shown clearly in Fig. 6 where we have plotted the pathlines of the flow. The plus signs are the most recent positions of the vertices and the dots are the positions at three previous equal periods of time. The plus signs can be regarded as arrow heads. We see the development of two large counter-rotating Taylor vortex cells. The wavelengths of the vortex cells is 4 cm as predicted by the theory.

Figures 3, 4 and 6 can be directly compared to the experimental work of Donnelly and Fultz[6] (see Fig. 7). They ejected dye from the inner cylinder and took a remarkable series of photographs showing the transition from laminar flow to fully developed Taylor vortex flow. Their work is also illustrated in Chandrasekhar.[4]

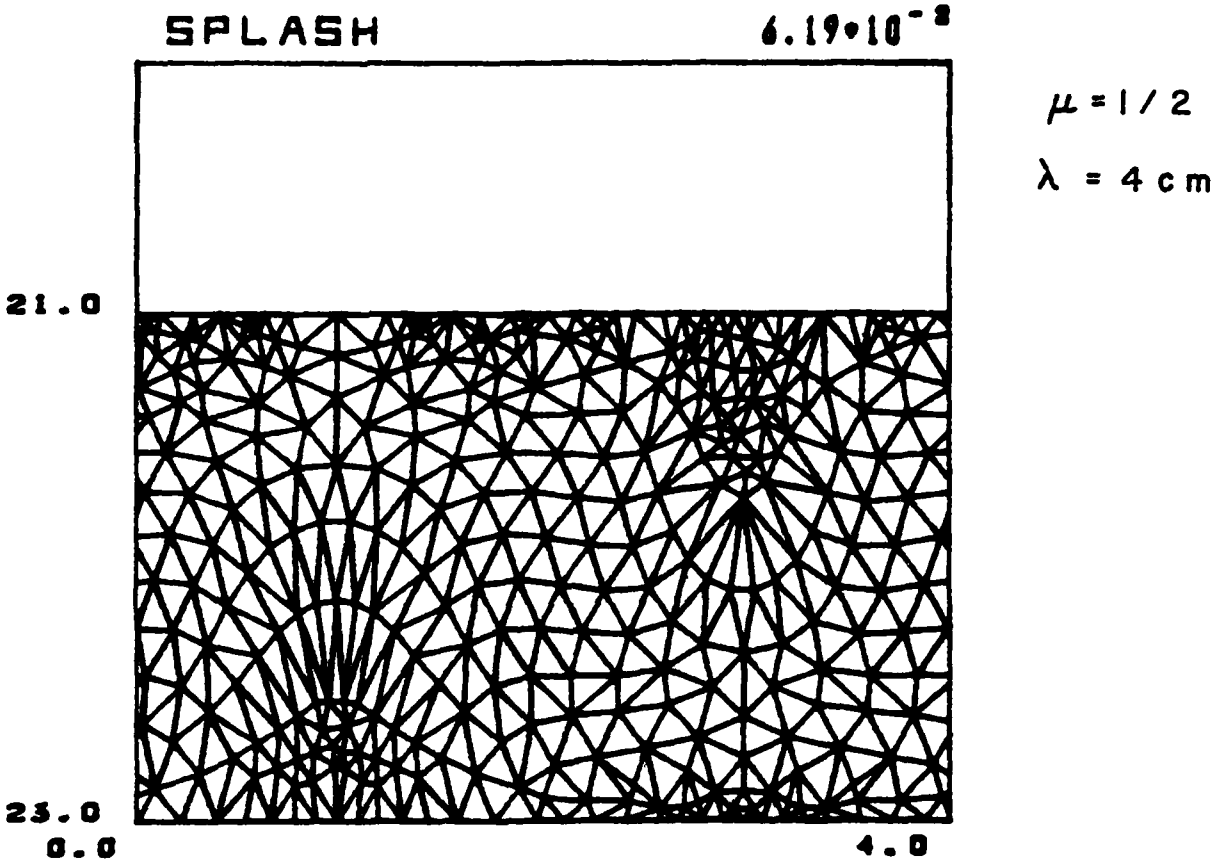

Fig. 4 — The grid after a revolution of the cylinders for Case I ($\mu = 1/2$, $\eta = 0.91$). The fluid is rolling up into a Taylor vortex.

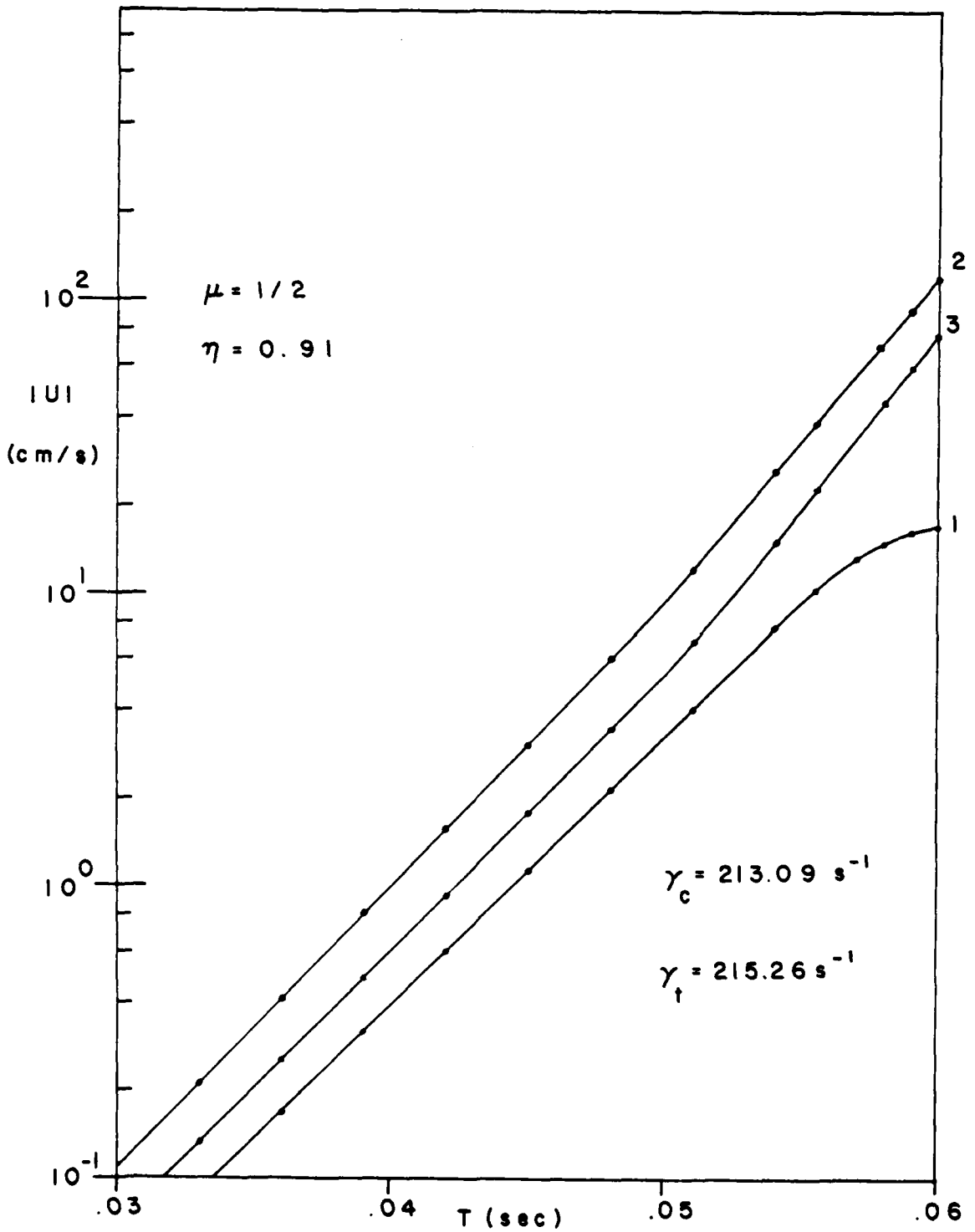

Fig. 5 — The r-component of the velocity for vertices 1, 2 and 3 as a function of time for Case I

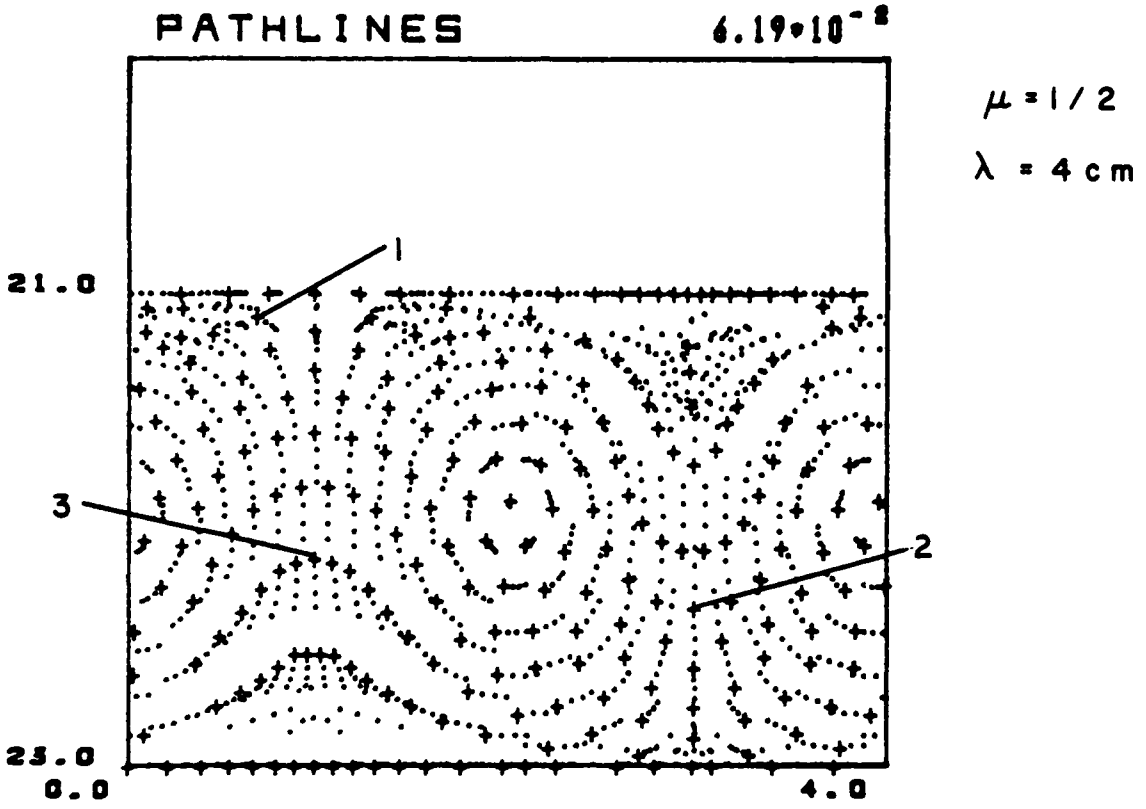

Fig. 6 — Pathlines for Case I. The + signs are the most recent positions of the vertices and the dots are the positions at three previous equal periods of time. The center vortex has a clockwise rotation. Vertices 1, 2 and 3 are noted.

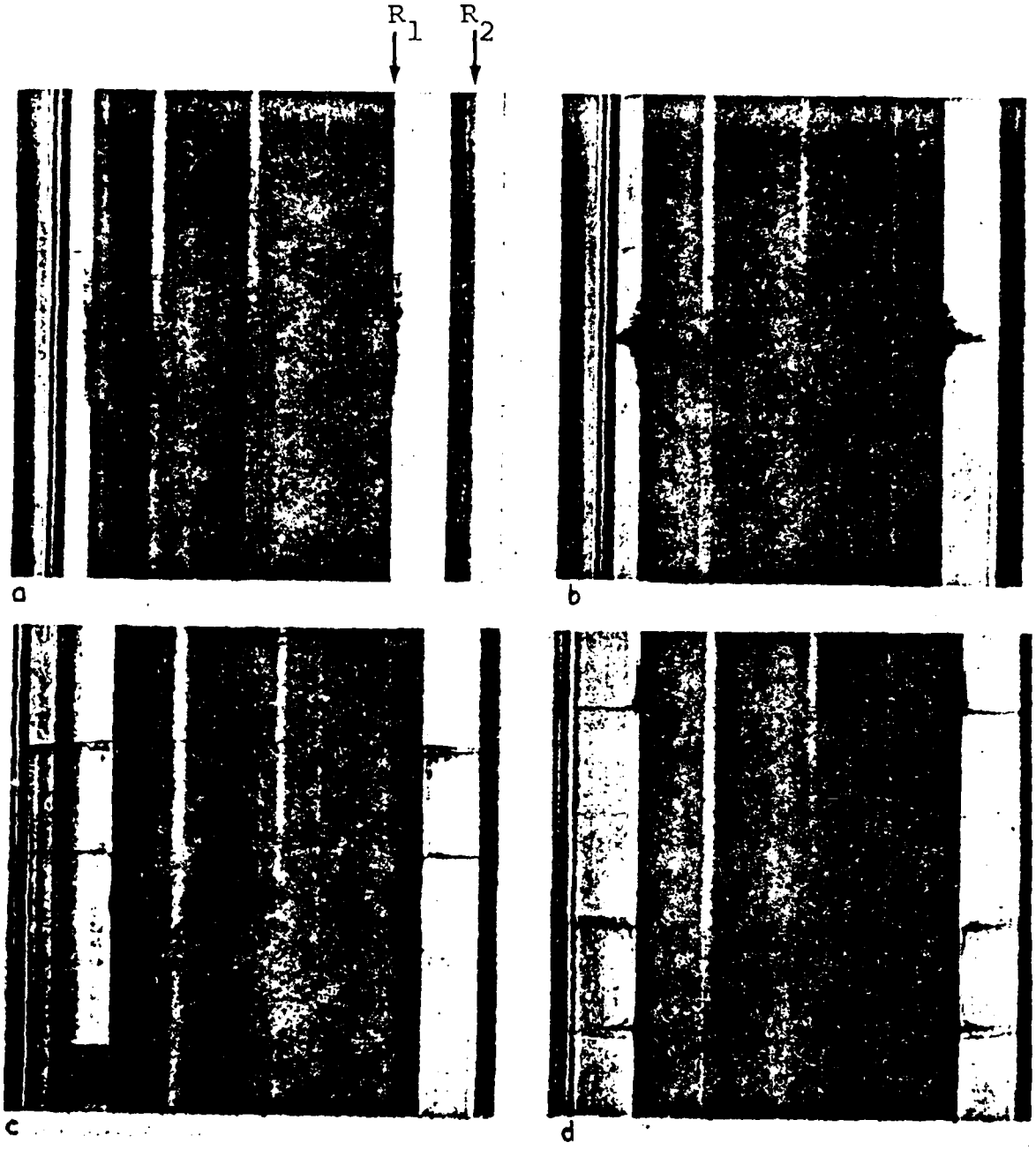

R-088

The onset of instability with the outer cylinder at rest, $\mu = 0$, $P_c = 4{\cdot}491$ sec: (*a*) laminar flow, $P = 4{\cdot}500$ sec; (*b*) beginning of radial motion at $P = 4{\cdot}483$ sec; (*c*) Appearance of cells with the outer cylinder at rest; cells at marginal stability, $P = P_c = 4{\cdot}466$ sec; (*d*) Appearance of cells with cylinders rotating in the same direction: $P = P_c = 3{\cdot}844$ sec, $\mu = 0{\cdot}1164$.

Fig. 7 — Photographs showing the transition from laminar Couette flow to fully developed Taylor-vortex flow with the outer cylinder at rest. Dye is ejected from the inner cylinder. R.J. Donnelly and D. Fultz, Proc. Roy Soc. A 258, 101 (1960). Used by permission.

For Case II, the outer cylinder is at rest, $\mu = 0$, and the system length has been increased to 12 cm. R_1, R_2, Ω_1 and k are the same as for Case I. Since the wavelength of the perturbation is 4 cm, six Taylor cells should develop. This is illustrated in Fig. 8 where we have plotted contours of constant circulation. The plus sign indicates flow in the clockwise direction.

The case for which the cylinders are rotating in the opposite direction is particularly interesting. Theory predicts that only the inner region of fluid should be unstable as it is only in this region that the angular momentum is decreasing. For Case III we have

$$R_1 = 41 \text{ cm}, \; R_2 = 45 \text{ cm},$$

$$z_N = 8 \text{ cm}, \; k = \pi$$

$$\Omega_1 = 40\pi s^{-1}, \; \mu = -0.87.$$

This choice of μ gives zero angular momentum at the center of the gap. The constant circulation contours are shown in Fig. 9. As predicted, four counter-rotating vortex cells appear in the inner half of the fluid while the outer half of the fluid remains stable. This figure can also be directly compared with the photographs of the experimental work of Donnelly and Fultz[15] (Fig. 10).

The numerical results for all the cases are summarized in table form in Fig. 11. The computational growth rates are in very good agreement with the theoretical growth rates with errors on the order of 1%. Note that for $\mu = 1$ the fluid is stable and γ is the oscillation frequency of the perturbed velocity.

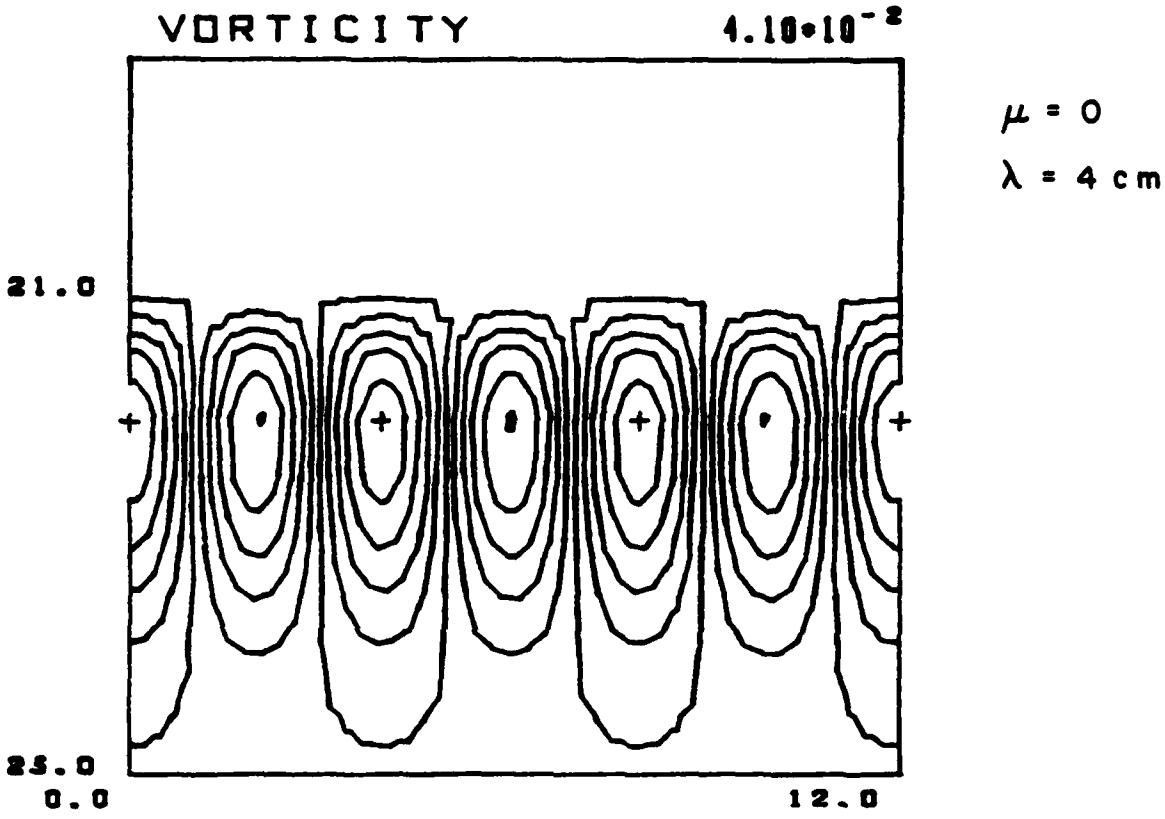

Fig. 8 — Contours of constant circulation ($\Gamma = \oint \underline{v} \cdot d\ell$) for Case II ($\mu = 0$, $\eta = 0.91$)

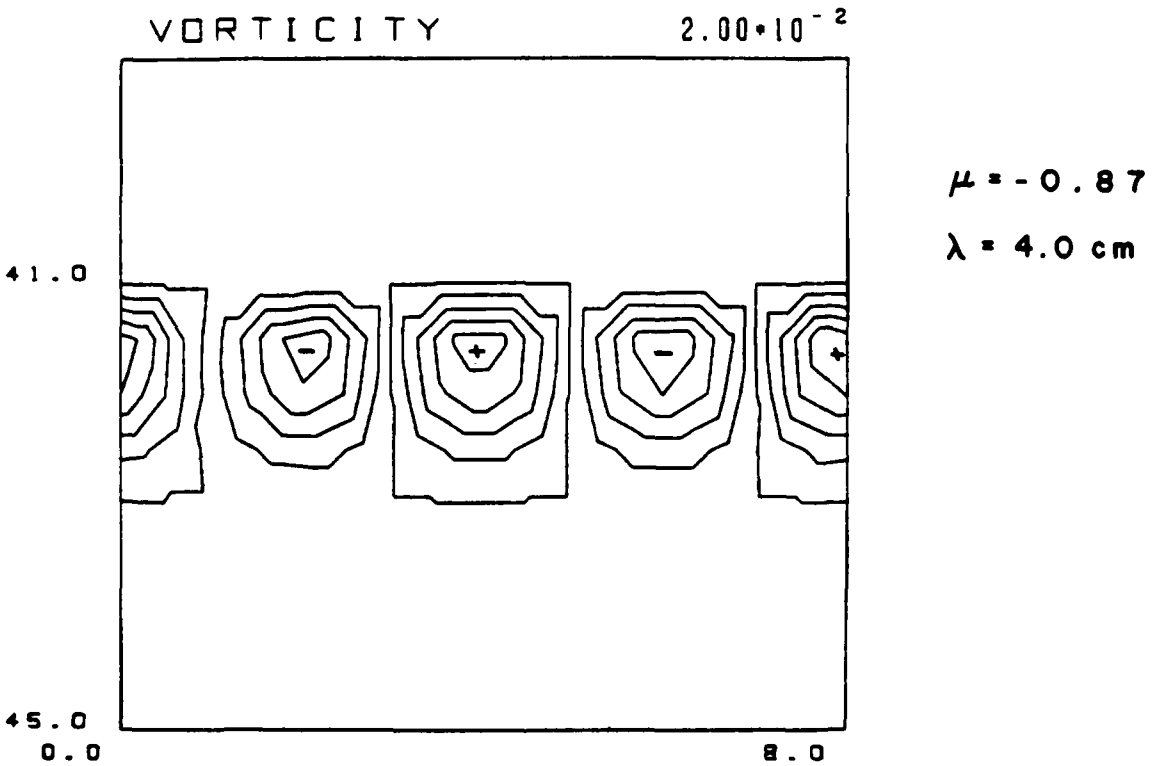

Fig. 9 — Contours of constant circulation for Case III ($\mu = -0.87$, $\eta = 0.91$)

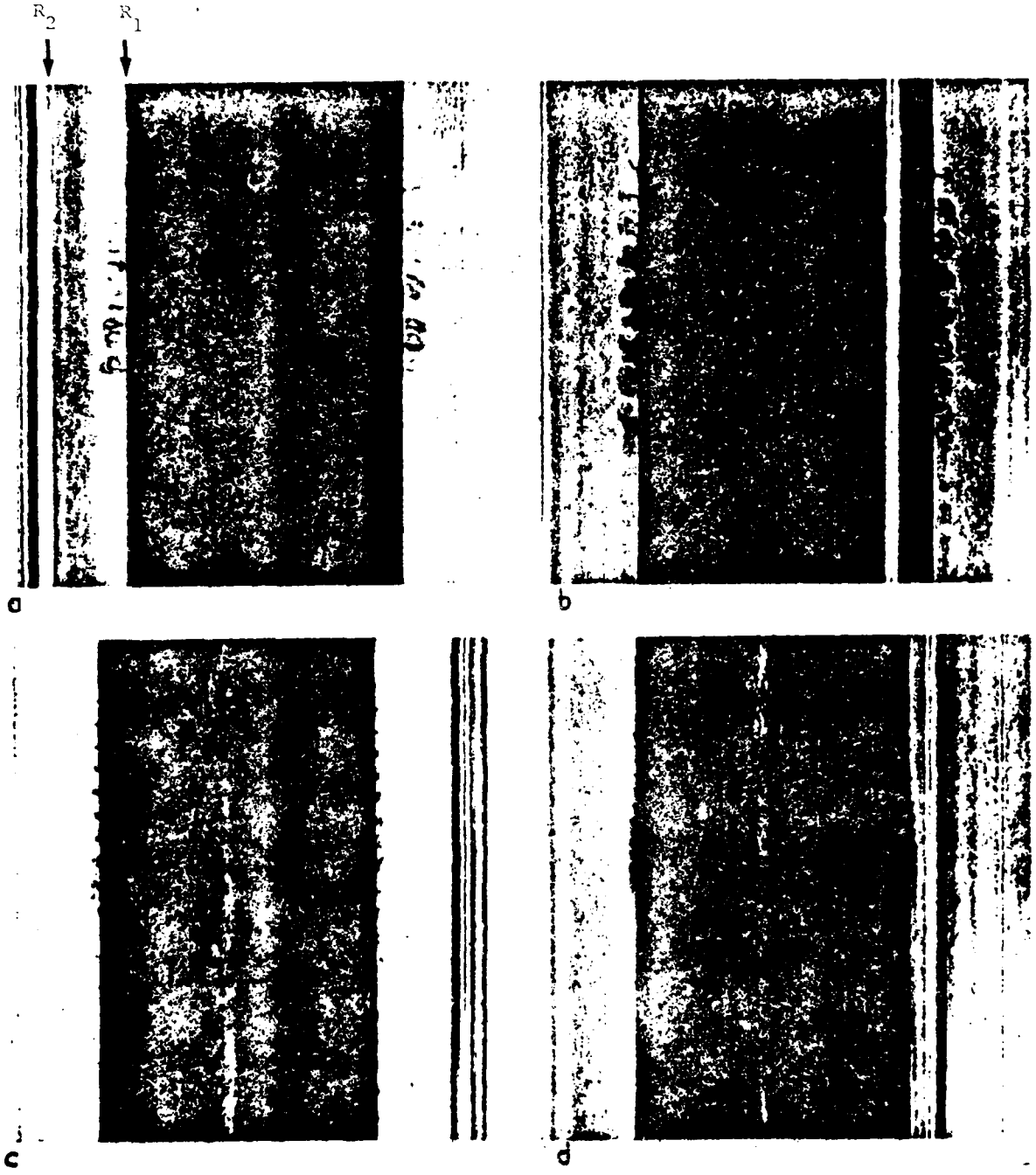

Photographs of cells with cylinders ($\eta = \frac{1}{2}$) rotating in opposite directions:
(*a*) $\mu = -2{\cdot}44$; (*b*) $\mu = -3{\cdot}02$; (*c*) $\mu = -5{\cdot}86$; and (*d*) $\mu = -6{\cdot}83$.

Fig. 10 — Photographs of fully developed Taylor vortices for counter-rotating cylinders.
R.J. Donnelly and D. Fultz, op cit. used by permission.

NUMERICAL RESULTS

COUETTE FLOW

$\eta = 0.91$

μ	Ω_1 (rad/s)	k	γ_c (sec^{-1})	γ_t (sec^{-1})
1	20π	$\pi/3$	69.81	69.74
1/2	20π	$\pi/3$	79.22	79.97
1/2	40π	$\pi/2$	213.09	215.26
0	40π	$\pi/2$	280.84	282.67
-0.87	40π	π	396.52	402.75

Fig. 11 — Comparison of computational growth rates with growth rates obtained from linear theory for various initial conditions

VII. Summary and Conclusions

We have developed a 2 1/2 dimensional, Lagrangian, hydrodynamic model designed for the simulation of transient rotational flow phenomena. The model uses as a finite difference mesh a general connectivity triangular grid. The advantages of this model are numerous:

1) Complicated geometries, interfaces and free surfaces can be treated with a minimum of difficulty.
2) The resolution across the mesh is highly variable.
3) The mesh can be restructured to preserve the numerical accuracy of the simulation.
4) No numerical vorticity is generated.
5) The gradient operator, as a triangle function, is exact in the linear approximation.
6) The integral operator, as a vertex function, is exact in the linear approximation.

We have applied this model to the study of the transition of laminar Couette flow to Taylor vortex flow with a high degree of success. The computational growth rates are in excellent agreement with the theory.

For the results presented here the code has not been run long enough to achieve steady-state Taylor-vortex flow. However, with respect to the transition to Taylor-vortex flow we find that a vortex signature appears very early in the run when the system is still in the linear regime. By this we mean that contours of constant circulation show uniformly spaced vortices when the perturbed velocities are on the order of 10^{-6} cm/sec. [$V_\theta \sim 0(10^3$ cm/sec)]. These vortices then increase in strength but maintain their shape and spacing.

In these calculations we have perturbed the system at only one wavelength corresponding to the predicted wavenumber for the steady-state Taylor vortices. Although the wavenumber is therefore not expected to change, it is surprising to find that the flow throughout the cylinder gap is established during the linear regime in exactly the nonlinear flow pattern. As evidenced by the case of the counter-rotating cylinders, this flow is not evident à priori. The transition to Taylor-vortex flow from laminar Couette flow is strickly speaking nonexistent — the linear flow is only strengthened. Whether any consequences of this simple transitioning are evident in the more complicated cases of viscid flow a d the perturbations of many wavenumbers will be investigated in future calculations.

Two code modifications are necessary for these calculations to be compared with experiments; the addition of viscosity (see Appendix A) and the improvement of some grid restructuring algorithms. In order to preserve numerical accuracy when the grid becomes highly distorted vertex additions and deletions must be made. We have now developed vertex addition/deletion algorithms which conserve divergence, curl, linear momentum, angular momentum and vorticity generation. These algorithms are now being incorporated into the code to allow the calculation to proceed further into the fully nonlinear regime while preserving second-order accuracy. These vertex addition/delection algorithms do not affect the results presented here.

The inclusion of viscosity and the new restructuring algorithms will enable a direct comparison between the computational results and the experimental results to be made. This would entail calculating the torques required to maintain the cylinders in motion and the critical Taylor number, the ratio of the destabilizing centrifugal force and the opposed radial

viscous force. These calculations of the fully developed nonlinear steady-state Taylor-vortex flow will be discussed in a future report.

Appendix A

Consider the viscid equations of motion written in our pseudo-Cartesian format

$$\frac{du}{dt} = -\frac{1}{\rho}\frac{\partial p}{\partial r} + \frac{v^2}{r} + \frac{\mu}{\rho}\left[2\frac{\partial}{\partial r}\left(\frac{\partial u}{\partial r}\right) + \frac{\partial}{\partial z}\left(\frac{\partial u}{\partial z} + \frac{\partial w}{\partial r}\right) + \frac{2}{r}\left(\frac{\partial u}{\partial r} - \frac{u}{r}\right)\right] , \quad \text{(A-1)}$$

$$\frac{dw}{dt} = -\frac{1}{\rho}\frac{\partial p}{\partial z} + \frac{\mu}{\rho}\left\{2\frac{\partial}{\partial z}\left[\frac{\partial w}{\partial z}\right] + \frac{1}{r}\frac{\partial}{\partial r}\left[r\left(\frac{\partial u}{\partial z} + \frac{\partial w}{\partial r}\right)\right]\right\} \quad \text{(A-2)}$$

and

$$\frac{dL}{dt} = r\mu\left[\frac{\partial^2 v}{\partial z^2} + \frac{\partial}{\partial r}\left(\frac{\partial v}{\partial r} - \frac{v}{r}\right) + \frac{2}{r}\left(\frac{\partial v}{\partial r} - \frac{v}{r}\right)\right] . \quad \text{(A-3)}$$

The coefficient of viscosity μ is considered a constant. Equations A-1 and A-2 can be combined to give

$$\frac{d\underline{u}}{dt} = -\frac{1}{\rho}\nabla p - 1/2L^2\nabla\frac{1}{r^2} - \frac{\mu}{\rho}\frac{1}{r}\nabla\times(r\underline{\omega}) , \quad \text{(A-4)}$$

where $\underline{\omega}$ is the theta component of vorticity

$$\underline{\omega} = \omega_\theta \hat{e}_\theta = \nabla\times\underline{u} .$$

ω_θ is a vertex function which is easily determined by calculating the circulation about a vertex

$$\omega_{\theta_i} = \frac{1}{A_i}\oint \underline{u}\cdot d\underline{l} .$$

Equation A-3 can be cast into the form of a diffusion equation for the angular momentum.

$$\frac{dL}{dt} = r\mu\nabla\cdot\left(\frac{1}{r}\nabla L\right) . \quad \text{(A-5)}$$

The finite differencing of this equation is discussed in detail in Ref. 10.

Acknowledgments

One of us (MHE) would like to extend his deep appreciation to A. L. Cooper for the many stimulating and rewarding discussions we had during the course of this project. This project was supported by the Office of Naval Research (Contract 61153N RR0140302) and the Naval Research Laboratory (Contract 61153N RR0230141).

References

1. M. J. Fritts and J. P. Boris, J. Comp. Phys. 31, 173 (1979); M. J. Fritts and J. P. Boris, "Solution of Transient Problems in Free-Surface Hydrodynamics," NRL Memorandum Report 3446 (1977).
2. Arnold L. Cooper, personal communication.
3. G. I. Taylor, Phil. Trans. A 223, 289 (1923).
4. S. Chandrasekhar, Hydrodynamic and Hydromagnetic Stability, Clarendon Press, 428 (1961).
5. J. L. Synge, Trans. of the Roy. Soc. of Canada 27, 1 (1933).
6. R. J. Donnelly and D. Fultz, Proc. Roy. Soc. A 258, (1960).
7. D. Coles, J. Fluid Mech. 21, 385 (1965).
8. A. Barcilon et al., J. Fluid Mech. 94, 453 (1979).
9. A. M. Winslow, J. Comp. Phys. 1, 149 (1966).
10. M. H. Emery and N. K. Winsor, "A Fully Two-Dimensional Equilibrium and Transport Model of the Poloidal Divertor," NRL Memorandum Report 4498 (1981). (Submitted to J. Comp. Phys.)
11. M. J. Fritts, "Transient Free-Surface Hydrodynamics," NRL Memorandum Report 365 (1977).
12. M. J. Fritts, "A Numerical Study of Free-Surface Waves," Science App., Inc. Report SAI-76-S28-WA (1976).
13. Lord Rayleigh, Proc. Roy. Soc. A 93, 148 (1916).
14. W. H. Reid, J. Math Analysis and Applications 1, 411 (1960).